A mechanical model of the four-point end notched flexure (4ENF) test based on an elastic-brittle interface

Stefano Bennati[1,a], Luca Taglialegne[1,b] and Paolo S. Valvo[1,c]

[1]Department of Structural Engineering, University of Pisa, Via Diotisalvi 2, I-56126 Pisa, Italy

[a]s.bennati@ing.unipi.it, [b]luca.taglialegne@gmail.com, [c]p.valvo@ing.unipi.it

Keywords: composite laminates, delamination, 4-point end notched flexure test, elastic interface.

Abstract. The paper introduces a mechanical model of the four-point end notched flexure (4ENF) test used to assess the mode II interlaminar fracture toughness in laminated specimens under stable crack-growth conditions. The model considers the specimen as an assemblage of two sublaminates, partly bonded together by a deformable interface. Each sublaminate is modelled as an elastic orthotropic beam, while the interface consists of a continuous distribution of normal and tangential linearly elastic-brittle springs. The mechanical behaviour of the system is described by a set of twenty-four differential equations, endowed with suitable boundary conditions. The original problem is split into two sub-problems, considering separately the symmetric and antisymmetric loads. The explicit solution to the problem is deduced for the internal forces and interlaminar stresses. Moreover, the energy release rate and compliance are determined. The predictions of the model are compared to theoretical and experimental results available in the literature.

Introduction

The separation between the laminae that make up a fibre-reinforced composite laminate, commonly known as delamination, is a major failure mode for this class of materials. Similar decohesion phenomena are observed also in thin films, glued joints, sandwich panels, laminated wood, layered glass, and other layered materials in all fields of technology [1]. In general, delamination growth involves simultaneously the three modes of crack propagation: opening (I), sliding (II), and tearing (III) [2]. Therefore, specific laboratory tests have been developed for assessing interlaminar toughness in each fracture mode and their combinations [3]. The end notched flexure (ENF) was the first test proposed for measuring pure mode II toughness, but it suffers from unstable crack growth. In order to obtain stable crack growth, Martin and Davidson [4] proposed the four-point end notched flexure (4ENF) test, where the load is applied to the specimen through a loading platen (Fig. 1).

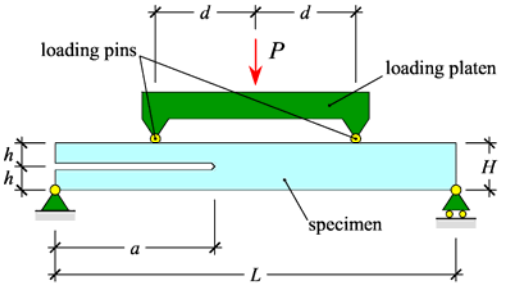

Figure 1 – Scheme of the four-point end notched flexure test.

In [4] the compliance and energy release rate (ERR) were determined resorting to a simple beam-theory (SBT) model. Subsequently, Davidson and Sun investigated the effects of friction and geometric nonlinearities by means of numerical models [5]. Actually, the SBT model of the 4ENF

test turns out to be inadequate for describing some features of real specimens, for instance it underestimates the compliance. In this paper, an enhanced beam-theory (EBT) model is introduced, whereby the specimen is represented as an assemblage of two sublaminates, partly connected by a deformable interface. The sublaminates are modelled as extensible, flexible and shear-deformable beams. The interface is regarded as a continuous distribution of springs acting along both the normal and tangential directions. Many similar interface models have been proposed in literature, for instance for the DCB [6], ENF [7] and ADCB [8] specimens.

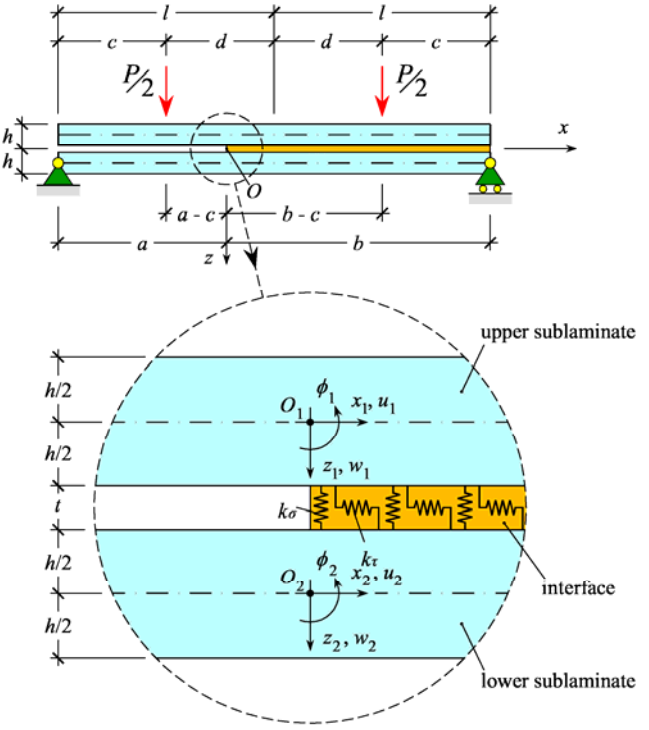

Figure 2 – The enhanced beam model of the 4ENF test, with a detail of the elastic interface.

Formulation of the problem

The model. The model is schematically represented in Fig. 2. Let $L = 2l$, $H = 2h$, and B be respectively the specimen's length, thickness, and width (not shown in the figure); let a be the delamination length. The lower sublaminate is simply supported at its ends, while two equal loads of intensity $P/2$ act on the upper sublaminate at distances d from the mid-span section. Moreover, we define the lengths $b = L - a$ and $c = l - d$. A rectangular coordinate system $Oxyz$ is fixed with the origin O at the crack tip, the x-axis parallel to the axial direction of the specimen and the z-axis pointing downwards. Let u_α and w_α denote the mid-plane displacements of the sublaminates along the x and z-axes, respectively, and let ϕ_α be the (positive if counter-clockwise) cross-sectional rotations (the subscript α assumes the values 1 or 2 to refer, respectively, to the upper and lower sublaminates). Let E_x, E_z and G_{zx} be the elasticity moduli of the laminate. The sublaminates are connected by a deformable interface, consisting of a continuous distribution of normal and tangential springs, whose elastic constants are k_σ and k_τ, respectively. The thickness of the interface, t, is assumed to be as small as needed to be negligible in solving the problem.

The differential problem. The equilibrium equations for the two sublaminates are

$$\frac{dN_\alpha}{dx}+n_\alpha=0,\quad \frac{dQ_\alpha}{dx}+q_\alpha=0,\quad \frac{dM_\alpha}{dx}+m_\alpha-Q_\alpha=0,\qquad \alpha=1,2, \tag{1}$$

where N_α, Q_α, and M_α are the axial force, shear force, and bending moment, and

$$n_1=-n_2=\begin{cases}0, & x<0,\\ B\,\tau, & x\geq 0,\end{cases}\qquad q_1=-q_2=\begin{cases}0, & x<0,\\ B\,\sigma, & x\geq 0,\end{cases}\qquad m_1=m_2=\begin{cases}0, & x<0,\\ Bh\,\tau/2, & x\geq 0,\end{cases} \tag{2}$$

are distributed loads and couples related to the normal and tangential interfacial stresses,

$$\sigma=k_\sigma\,\Delta w,\quad \tau=k_\tau\,\Delta u\,, \tag{3}$$

which, in turn, are proportional to the transverse and axial relative displacements at the interface,

$$\Delta w=w_2-w_1,\quad \Delta u=u_2-u_1-\frac{h}{2}(\phi_1+\phi_2)\,. \tag{4}$$

The constitutive laws for the sublaminates can be written as

$$N_\alpha=BA_\alpha\varepsilon_\alpha,\quad Q_\alpha=BC_\alpha\gamma_\alpha,\quad M_\alpha=BD_\alpha\kappa_\alpha,\qquad \alpha=1,2, \tag{5}$$

where $A_1=A_2=E_x h$, $C_1=C_2=5G_{zx}h/6$, and $D_1=D_2=E_x h^3/12$ are respectively the extensional, shearing and bending stiffnesses, and

$$\varepsilon_\alpha=\frac{du_\alpha}{dx},\quad \gamma_\alpha=\phi_\alpha+\frac{dw_\alpha}{dx},\quad \kappa_\alpha=\frac{d\phi_\alpha}{dx},\qquad \alpha=1,2, \tag{6}$$

are respectively the axial strain, shear strain, and curvature of the sublaminates.

By substituting Eqs. 2-6 into Eq. 1, we obtain six differential equations for each of the four intervals defined between the following values of the abscissa x:

$$x_A=-a,\quad x_B=l-d-a=c-a,\quad x_C=0,\quad x_D=l+d-a=b-c,\quad x_E=L-a=b. \tag{7}$$

So, a set of twenty-four governing differential equations is obtained, endowed with appropriate boundary conditions. The details of the analytical solution are here omitted and will be presented in the full paper. In what follows only the solution strategy and the main results are illustrated.

Analytical solution

Solution strategy. The stated problem is conveniently split into two subproblems where the symmetric and antisymmetric parts of the loads are applied separately (Fig. 3). It can be easily proved that the symmetric load system only produces normal interfacial stresses, so it is related to pure mode I fracture; conversely, the antisymmetric load system is responsible only for tangential interfacial stresses, so it corresponds to pure mode II fracture. Actually, despite the 4ENF is considered a pure mode II test, an additional mode I contribution to the ERR comes out naturally by solving the proposed model. However, for material properties corresponding to ordinary composite laminates, this mode I contribution turns out to be mostly negligible. Therefore, in what follows we restrict our attention to the antisymmetric problem only (Fig. 4).

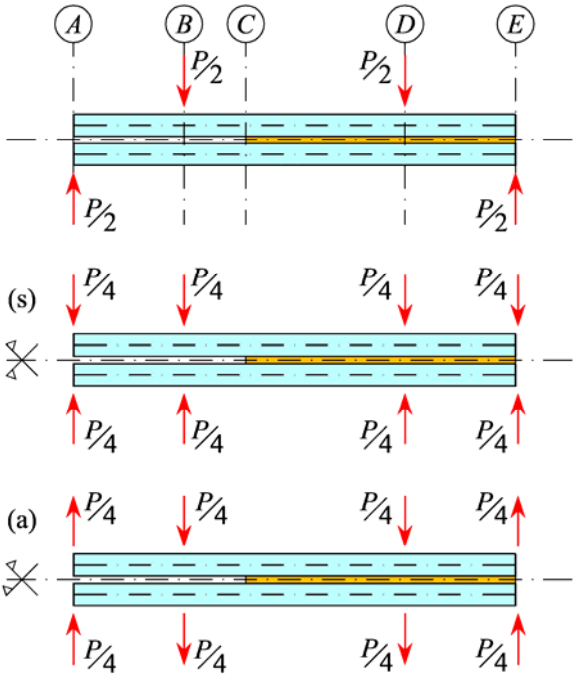

Figure 3 – Splitting of the original problem into symmetric and antisymmetric sub-problems.

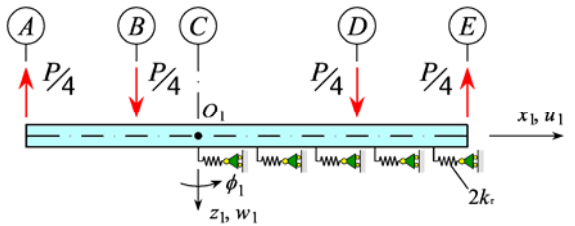

Figure 4 – Antisymmetric system (upper sublaminate).

Internal forces. Integrating the governing set of differential equations with the boundary conditions, we obtain explicit expressions for the internal forces in the sublaminates,

$$N_1(x) = -N_2(x) = \begin{cases} 0, & x \in [x_A, x_C], \\ -\dfrac{3P}{8h}\left[c\,(1-\cosh\gamma x) + \left(c\coth\gamma b - \dfrac{\sinh\gamma c}{\gamma \sinh\gamma b} \right)\sinh\gamma x \right], & x \in [x_C, x_D], \\ -\dfrac{3P}{8h}\left\{ b - x - \left[c + \dfrac{\sinh\gamma(b-c)}{\gamma} \right](\cosh x - \coth\gamma b \sinh\gamma x) \right\}, & x \in [x_D, x_E], \end{cases} \quad (8)$$

for the axial forces, where $\gamma^2 = 8k_\tau / E_x h$,

$$Q_1(x) = Q_2(x) = \begin{cases} \dfrac{P}{4}, & x \in [x_A, x_B], \\ 0 & x \in [x_B, x_D], \\ -\dfrac{P}{4}, & x \in [x_D, x_E], \end{cases} \tag{9}$$

for the shear forces, and lastly,

$$M_1(x) = M_2(x) = \begin{cases} \dfrac{P}{4}(a+x), & x \in [x_A, x_B], \\ \dfrac{P}{4}c, & x \in [x_B, x_C], \\ \dfrac{P}{16}\left[c\,(1+3\cosh\gamma x) - 3\left(c\coth\gamma b - \dfrac{\sinh\gamma c}{\gamma \sinh\gamma b}\right)\sinh\gamma x \right], & x \in [x_C, x_D], \\ \dfrac{P}{16}\left\{ b - x + 3\left[c + \dfrac{\sinh\gamma(b-c)}{\gamma}\right](\cosh\gamma x - \coth\gamma b \sinh\gamma x)\right\}, & x \in [x_D, x_E], \end{cases} \tag{10}$$

for the bending moments.

Interfacial stress. Hence, remembering Eqs. 1 and 2, we obtain the tangential interfacial stress,

$$\tau(x) = \begin{cases} \dfrac{3P}{8Bh}\left[\left(\gamma c \coth\gamma b - \dfrac{\sinh\gamma c}{\sinh\gamma b}\right)\cosh\gamma x - \gamma c \sinh\gamma x \right], & x \in [x_C, x_D], \\ -\dfrac{3P}{8Bh}\left\{ 1 - [\gamma c + \sinh\gamma(b-c)](\coth\gamma b \cosh\gamma x - \sinh\gamma x)\right\}, & x \in [x_D, x_E]. \end{cases} \tag{11}$$

In particular, at the crack tip

$$\tau_C = \tau(x)\big|_{x=0} = \frac{3P}{8Bh}\frac{\gamma c\cosh\gamma b - \sinh\gamma c}{\sinh\gamma b}. \tag{12}$$

Energy release rate. The energy release rate is immediately determined from Eq. 12

$$G_{\mathrm{II}} = \frac{\tau_C^{\,2}}{2k_\tau} = G_{\mathrm{II,SBT}}(\coth\gamma b - \frac{\sinh\gamma c}{\gamma c \sinh\gamma b})^2 = G - G_{\mathrm{I}} \cong G\,, \tag{13}$$

where

$$G_{\mathrm{II,SBT}} = \frac{9P^2(l-d)^2}{16\,E_{\mathrm{x}}B^2h^3} = \frac{9P^2c^2}{16\,E_{\mathrm{x}}B^2h^3} \tag{14}$$

is the energy release rate deduced from the simple beam-theory model.

Compliance. By integrating the following expression

$$G = \frac{P^2}{2B}\frac{dC}{da}, \tag{15}$$

where G is given by Eq. 13, we obtain the compliance of the specimen as

$$C = C_{\mathrm{SBT}} + C_{\mathrm{interf}} + C_{\mathrm{shear}}, \tag{16}$$

where

$$C_{\mathrm{SBT}} = \frac{(l-d)^2}{8\,E_{\mathrm{x}}Bh^3}[9a - 4l + 10d)] \tag{17}$$

is the compliance stemming from the simple beam-theory model,

$$C_{\mathrm{interf}} = \frac{9(l-d)^2}{8\,E_{\mathrm{x}}Bh^3}\,\frac{\cosh\gamma b + \dfrac{\sinh\gamma b - 2\sinh\gamma c}{\gamma c} - \dfrac{\sinh\gamma c \sinh\gamma(b-c)}{\gamma^2 c^2}}{\gamma \sinh\gamma b} \tag{18}$$

is the contribution due to the deformability of the elastic interface, and

$$C_{\mathrm{shear}} = \frac{3(l-d)}{10\,G_{\mathrm{zx}}Bh} \tag{19}$$

is the contribution due to the shear deformability of the sublaminates.

Application

By way of illustration, we now apply the proposed model to the case of a unidirectional carbon fibre/epoxy laminate, previously considered in an experimental study by Zile and Tamuzs [9]. Test specimens were produced by gluing together three 1.2 mm thick sheets of Sika CarboDur® S 512 by means of a Bison polyurethane power adhesive. In particular, the specimens considered have dimensions $L = 2l = 160$ mm, $H = 2h = 4.2$ mm, and $B = 13.2$ mm. The initial delamination length is $a_0 = 55$ mm and the distance of the loads from the mid-span section is $d = 40$ mm. The elastic moduli of the material are $E_{\mathrm{x}} = 165$ GPa, $E_{\mathrm{y}} = E_{\mathrm{z}} = 9$ GPa, $G_{\mathrm{xy}} = 5$ GPa $\approx G_{\mathrm{zx}}$.

The values of the elastic constants of the interface should be assigned in order to account for the localised deformation occurring at the crack tip, neglected by the SBT model. Generally speaking, these constants are related to the elastic moduli of the laminate in the z-direction and to the mechanical properties of the adhesive layers (if present). These constants can be estimated by calibrating the analytical model with the results of experimental tests or numerical models. Here, we have matched the compliance deduced from our model with that stemming from the tests and found $k_\tau = 310$ N/mm^3. This value, obtained for $a = a_0$, has then been adopted in all calculations.

Fig. 5 shows the internal forces in the upper sublaminate, as given by Eqs. 8-10, as functions of the abscissa, x, ranging over the whole specimen length from $x_A = -55$ mm to $x_E = 105$ mm. A load $P = 500$ N is here considered, slightly below the value measured at crack growth initiation [9]. The axial force in the sublaminate, N_1, is zero from the left-hand end of the specimen, x_A, to the crack tip, $x_C = 0$ mm; it then becomes negative (the upper sublaminate is compressed, while the lower one undergoes traction) and finally goes to zero at the right-hand end of the specimen, x_E. A different trend is observed for the shear force, Q_1, which is constant, equal to $P / 4 = 125$ N, from x_A to the application point of the first load, $x_B = -15$ mm; it is equal to zero from x_B to the application point of the second load, $x_D = 65$ mm; it is again constant, equal to $-P / 4 = -125$ N, from x_D to x_E. A more complex behaviour is observed for the bending moment, M_1, which has a linear trend from x_A to x_B; it is constant, equal to $Pc / 4 = 5000$ N mm, from x_B to x_C; it then shows a non-linear trend with a local maximum at x_D, where the second load is applied, and finally goes to zero at x_E.

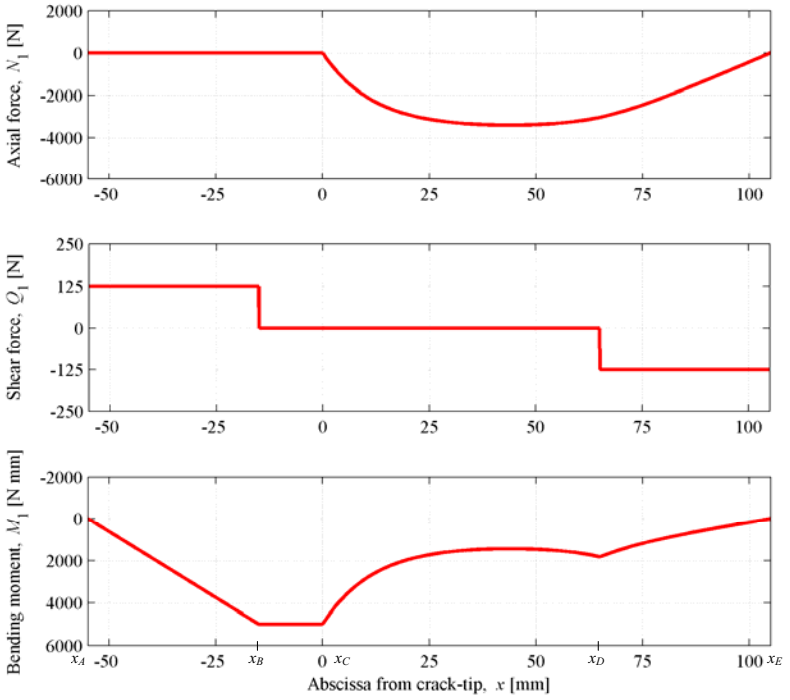

Figure 5 – Internal forces in the upper sublaminate.

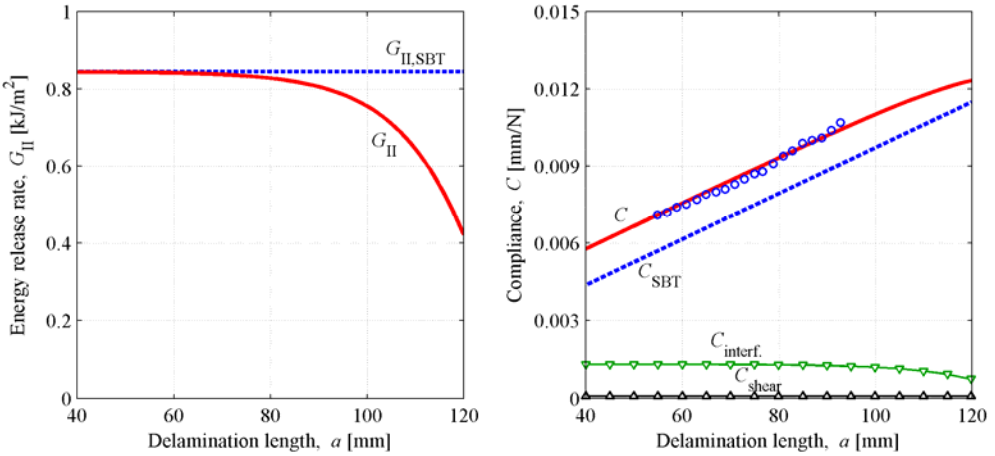

Figure 6 – Energy release rate and compliance (circles represent experimental data [9]).

Fig. 6 shows the energy release rate, G_{II}, and the compliance, C, as functions of the delamination length, a, as computed via Eqs. 13 and 16, respectively. For the sake of comparison, the same quantities as computed by the SBT model are also shown. The delamination length, a, ranges from 40 to 120 mm, corresponding to the crack tip moving from the left to the right load application points. A constant load $P = 500$ N is considered here. According to the EBT model, G_{II} turns out to be a decreasing function of a, while for the SBT model it has constant value. *So, the EBT model is able to explain why, during a test, it is necessary to increase the applied load in order to keep the*

delamination growing, even if we consider G_{IIc} *as constant material parameter. Instead, if experimental data are interpreted based on the SBT model, apparent R-curves are found where* G_{IIc} *is an increasing function of* a [9]. As far as the compliance is concerned, the figure shows the three contributions present in the right-hand side of Eq. 16 and experimental data from [9]. The contribution of shear deformability, C_{shear}, is very small and, moreover, is constant with respect to a, so it is expected to have no influence on the ERR. The compliance computed via the SBT model, C_{SBT}, underestimates the experimental results which, instead, are very well matched by our model including the contribution of the elastic interface, C_{interf}.

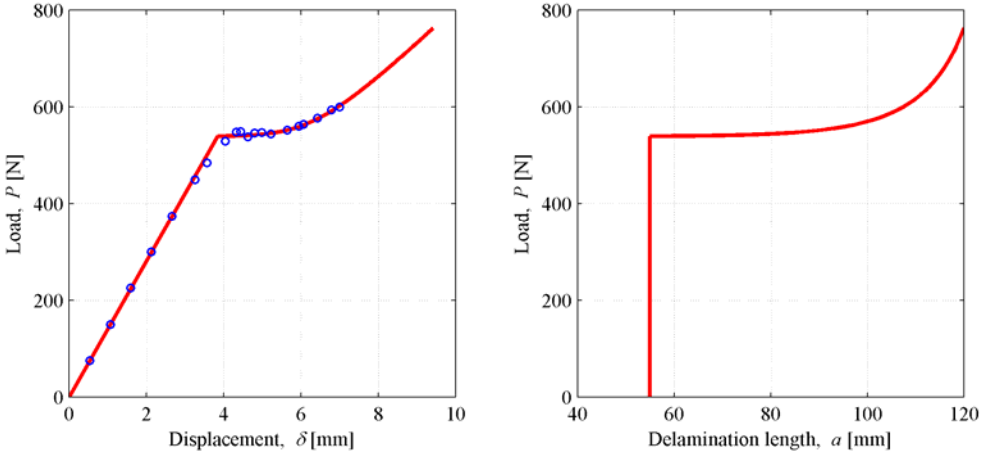

Figure 7 – Load vs. displacement and delamination length (circles represent experimental data [9]).

The specimen's response during a load test is summarised in Fig. 7, where the load, P, is plotted against the load application point displacement, δ, and delamination length, a. In both figures, the initial linear branches represent the response of the specimen prior to crack initiation. The curved, increasing branches represent the stage of crack growth, as predicted by our model by setting $G_{II} = G_{IIc} = 983.3$ J/m^2. This value is deduced from Eq. 13 for $P = P_c = 540$ N, which is the experimentally measured critical load. Contrary to the SBT model, the EBT model predicts an increase in the applied load under constant $G_{II} = G_{IIc}$, and is in very good agreement with the tests.

References

[1] T.E. Tay: Appl. Mech. Rev., Vol. 56 (2003), p. 1.

[2] K. Friedrich (editor): *Application of Fracture Mechanics to Composite Materials* (Elsevier, Amsterdam, 1989).

[3] D.F. Adams, L.A. Carlsson and R. Byron Pipes: *Experimental Characterization of Advanced Composite Materials – 3rd edition* (CRC Press, Boca Raton, 2003).

[4] R.H. Martin and B.D. Davidson: Plast. Rubber Compos., Vol. 28 (1999), p. 401.

[5] B.D. Davidson and X. Sun: Eng. Fract. Mech., Vol. 73 (2006), p. 1343.

[6] M.F. Kanninen: Int. J. Fract., Vol. 9 (1973), p. 83.

[7] W. Ding and M.T. Kortschot: Compos. Struct., Vol. 45 (1999), p. 271.

[8] S. Bennati, M. Colleluori, D. Corigliano and P.S. Valvo: submitted to Comp. Sci. Tech. (2008).

[9] E. Zile and V. Tamuzs: Mech. Compos. Mater., Vol. 41 (2005), p. 383.